Optics Letters

Plasmonic loss-mitigating broadband adiabatic polarizing beam splitter

GUANG YANG, ALEXANDER V. SERGIENKO, AND ABDOULAYE NDAO*

Department of Electrical and Computer Engineering & Photonics Center, Boston University, 8 Saint Mary's Street, Boston, Massachusetts 02215, USA
**Corresponding author: andao@bu.edu*

Received 19 May 2021; revised 19 November 2021; accepted 20 November 2021; posted 23 November 2021; published 25 January 2022

The intriguing analogy between quantum physics and optics has inspired the design of unconventional integrated photonics devices. In this paper, we numerically demonstrate a broadband integrated polarization beam splitter (PBS) by implementing the stimulated Raman adiabatic passage (STIRAP) technique in a three-waveguide plasmonic system. Our proposed PBS exhibits >250 nm transverse-magnetic (TM) bandwidth with <−40 dB extinction and >150 nm transverse-electric (TE) bandwidth with <−20 dB extinction, covering the entire S-, C-, and L-bands and part of the E-band. Moreover, near-lossless light transfer is achieved in our system despite the incorporation of a plasmonic hybrid waveguide because of the unique loss mitigating feature of the STIRAP scheme. Through this approach, various broadband integrated devices that were previously impossible can be realized, which will allow innovation in integrated optics.

https://doi.org/10.1364/OL.431887

Quantum physics processes can often be related to classical analogies in photonic systems [1] owing to similar mathematical forms of the Schrödinger equation and the paraxial Helmholtz equation. The stimulated Raman adiabatic passage (STIRAP) technique [2,3], originally developed for robust population transfer between three or more atomic or molecular energy levels, has found great applications in the manipulation and transfer of light in coupled waveguide systems. Since the initial proposal [4,5] and experimental demonstration [6] of STIRAP in waveguides, a variety of waveguide systems with versatile functionalities based on the STIRAP protocol have been reported, such as spectral filtering [7], beam splitting [8], and on-chip entanglement engineering [9]. Nevertheless, most current studies are limited to the consideration of non-dissipative dielectric systems. The generalization of this approach to open systems creates new opportunities for using plasmonics as well as the exceptional properties of non-Hermitian systems [10–12]. However, the adiabatic requirement of STIRAP, which impacts the device length, hinders such endeavors and limits their practicality. The use of artificial gain is considered in recent reports to cancel the dissipation [13] or accelerate the transfer [14]. However, such conditions are impractical over the required distances that are typically centimeters long. In this Letter, we adopt an alternative approach inspired by a generalized atomic STIRAP framework, where the transfer can be lossless if the loss (decay) only exists in the intermediate state of the three-level system [15]. We exploit this unique feature and use a hybrid plasmonic waveguide (HPWG) [16,17] as the intermediate state in our waveguide system. This enables the implementation of a robust integrated polarization beam splitter (PBS) based on the polarization selectivity of the plasmonic system. The advantage of using STIRAP principles here is twofold: it circumvents plasmonic losses and provides excellent operation bandwidth.

With the rapid development of photonic integrated circuits, more and more degrees of freedom, such as wavelength and polarization, can be manipulated on the same chip. An integrated broadband PBS, preferably executed using high-index-contrast structures, such as the state-of-the-art lithium niobate on insulator (LNOI) platform [18–21], is a highly needed device. However, the operational bandwidth supported by conventional designs, i.e., directional couplers, is limited to tens of nanometers, owing to the wavelength sensitivity of the interference effect [22]. Extending the operational bandwidth requires more sophisticated engineering of anisotropic structures, such as heteroanisotropic metamaterials [23] and cascaded interferometers with different birefringent paths [24]. While the performance of such devices is considered to be promising, the complexity of executing the sub-wavelength grating [23] and obtaining cascaded interferometers [24] is challenging, and the uncertainty in fabrication and device characterization increases. However, the STIRAP protocol has been used in simple dielectric-only waveguide systems and proven to offer large bandwidths [25–27]. However, these devices are based on low-index-contrast waveguide platforms that are incompatible with modern advanced integration technologies. Moreover, these dielectric-only designs require 3–5-cm-long devices and, sometimes, at least a five-waveguide system [26], because their operation relies on the material birefringence only.

Here, we propose a novel broadband PBS on a LNOI platform, which is based on a three-waveguide STIRAP scheme employing a plasmonic waveguide. To the best of our knowledge, this is the first STIRAP-based PBS reported in high-index-contrast integrated systems, featuring a short device length of 6 mm, which is 5-fold shorter than other STIRAP-PBS systems reported so far [25–27]. This approach opens fresh avenues for on-chip polarization control and introduces new principles of plasmonic system design and manipulation.

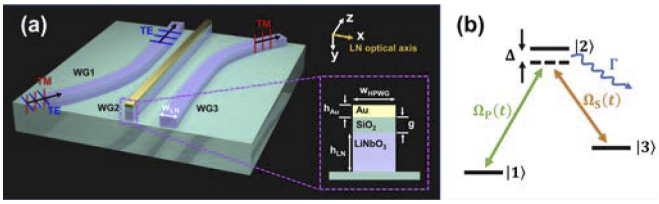

Fig. 1. (a) Schematic of the proposed device. The inset shows the cross-section of WG2 (the HPWG). (b) Three-level atomic system that is analogous to that shown in panel (a). The pulses Ω_p and Ω_s denote Rabi frequencies.

Figure 1 presents a schematic of the proposed PBS that illustrates its principle of operation. The device consists of three waveguides (WG1, WG2, WG3) made in X-cut thin-film lithium niobate ($h_{LN} = 375$ nm) on top of a silicon dioxide layer. The outer two waveguides (WG1 and WG3) are fully etched ridge waveguides with the same width of $w_{LN} = 900$ nm. The top cladding is air. Such parameters ensure single-mode operation within the designed bandwidth (approximately 1400–1700 nm). The HPWG in the middle (WG2) has a width of $w_{HPWG} = 300$ nm and comprises three layers: an LN ridge waveguide, a gold topping layer ($h_{Au} = 100$ nm), and a silicon dioxide interlayer (height $g = 80$ nm) between gold and LN. The electric field in this HPWG is mainly confined in the low index silicon dioxide layer, in analogy to a slot waveguide, while the plasmonic nature of this structure imposes transverse-magnetic (TM) polarization on the resultant mode. For a TM mode excited in the left waveguide (WG1), the light transfer in the three-waveguide system is analogous to the STIRAP process in a three-level atomic system [Fig. 1(b)], where the population initially in state $|1\rangle$ (or WG1) is transferred to state $|3\rangle$ (or WG3) via an intermediate state $|2\rangle$ (or WG2). The intermediate state $|2\rangle$ here is a decaying state (decay rate Γ), which reflects the lossy characteristic of WG2. In the waveguides system, the detuning Δ reflects the propagation constant mismatch between WG2 and WG1/WG3. In contrast to the three-waveguide coupling for the TM case, a transverse-electric (TE) mode starting in WG1 undergoes direct two-waveguide coupling between WG1 and WG3, because WG2 does not support TE polarization. A PBS effect is achieved because such cross-coupling of the TE mode is weak given the large separation between WG1 and WG3.

We describe the state evolution in the waveguide system and highlight the analogy with a population transfer process based on STIRAP (substitution $z \rightarrow t$ illustrates the equivalency with an atomic system):

$$i\frac{d}{dz}\mathbf{A} = \mathbf{H}\mathbf{A}, \tag{1}$$

where $\boldsymbol{A} = [a_1(z),\ a_2(z),\ a_3(z)]^T$ denotes the field distribution in WG1, WG2, and WG3. The focus of this study is the transfer of the TM mode, and all notations hereafter refer to TM unless otherwise specified. The interaction Hamiltonian $\mathbf{H}$ in a perturbation form can be written according to the coupled mode theory (CMT) [28]:

$$\begin{aligned}\mathbf{H} &\equiv \mathbf{H}^{(0)} + \mathbf{H}' \\ &= \begin{bmatrix} 0 & C_{12}(z) & 0 \\ C_{12}^*(z) & \Delta & C_{23}(z) \\ 0 & C_{23}^*(z) & 0 \end{bmatrix} + \begin{bmatrix} 0 & 0 & C_{13}(z) \\ 0 & i\Gamma & 0 \\ C_{13}^*(z) & 0 & 0 \end{bmatrix}.\end{aligned} \tag{2}$$

The unperturbed Hamiltonian, $\mathbf{H}^{(0)}$, represents a lossless system with detuning Δ in the intermediate level ($\Delta \equiv \Delta\beta = \beta_2 - \beta_1$ in the waveguide system), while the loss is accounted in the perturbation $\mathbf{H}'$. Here, C_{ij} denotes the coupling coefficient between WG-i and -j, and $C_{ij} = C_{ji}^*$ because $\mathbf{H}^{(0)}$ is lossless. The perturbation term $\mathbf{H}'$ is responsible for two effects: the loss from WG2 and the coupling between WG1 and WG3. The latter is exclusive to the waveguide system, as the direct transition between $|1\rangle$ and $|3\rangle$ in the atomic system is forbidden. Following the perturbation approach, we analyze our system starting from the zeroth-order term, $\mathbf{H}^{(0)}$, corresponding to a lossless STIRAP case. The full system is most conveniently understood when projected to the eigenstate basis of $\mathbf{H}^{(0)}$, often referred to as the adiabatic basis:

$$\begin{aligned}|\Psi_+^{(0)}\rangle &= \sin\phi\sin\theta|1\rangle + \cos\phi|2\rangle + \sin\phi\cos\theta|3\rangle \\ |\Psi_0^{(0)}\rangle &= \cos\theta|1\rangle - \sin\theta|3\rangle \\ |\Psi_-^{(0)}\rangle &= \cos\phi\sin\theta|1\rangle - \sin\phi|2\rangle + \cos\phi\cos\theta|3\rangle,\end{aligned} \tag{3}$$

with eigenvalues $\lambda_0^{(0)} = 0$ and $\lambda_\pm^{(0)} = \left(\Delta \pm \sqrt{\Delta^2 + 4C_0^2}\right)/2$, where $C_0(z) = \sqrt{|C_{12}(z)|^2 + |C_{23}(z)|^2}$. The parameters ϕ and θ are given by $\tan\theta(z) = C_{12}(z)/C_{23}(z)$ and $\tan 2\phi(z) = 2C_0(z)/\Delta$, respectively. These definitions lead to $\lambda_+^{(0)} \equiv C_0\cot\phi$ and $\lambda_-^{(0)} \equiv -C_0\tan\phi$.

Among the adiabatic states, of particular significance is $|\Psi_0^{(0)}\rangle$, also known as the dark state in STIRAP, because it does not involve the intermediate state $|2\rangle$. This highlights an important characteristic of ideal STIRAP: the population transfer takes place via $|2\rangle$ without populating $|2\rangle$ itself. In atomic STIRAP, the population transfer is enabled by the two pulses in the so-called counter-intuitive order, meaning the pulse connecting $|2\rangle$ and $|3\rangle$ precedes the pulse connecting $|1\rangle$ and $|2\rangle$. A similar configuration must be implemented in the waveguide system, such that for the initial state: $C_{12} \ll C_{23}$, $\theta_i \approx 0$, $|\Psi_0^{(0)}\rangle_i \approx |1\rangle$; and the final state: $C_{12} \gg C_{23}$; $\theta_f \approx \pi/2$; $|\Psi_0^{(0)}\rangle_f \approx |3\rangle$. Thus, an initial population in $|1\rangle$ has perfect overlap with $|\Psi_0^{(0)}\rangle_i$ and can thereby evolve into $|\Psi_0^{(0)}\rangle_f$ (or $|3\rangle$), provided that it remains in $|\Psi_0^{(0)}\rangle$ without crosstalk to $|\Psi_+^{(0)}\rangle$ and $|\Psi_-^{(0)}\rangle$. However, as $\mathbf{H}^{(0)}$ evolves, these *instantaneous* eigenstates become coupled, as can be seen from the corresponding Hamiltonian in the adiabatic basis:

$$\begin{aligned}\mathbf{H}_{adia} = &\begin{bmatrix} \lambda_+^{(0)} & i\dot\theta\sin\phi & i\dot\phi \\ -i\dot\theta\sin\phi & \lambda_0^{(0)} & -i\dot\theta\cos\phi \\ -i\dot\phi & i\dot\theta\cos\phi & \lambda_-^{(0)} \end{bmatrix} \\ &+ \begin{bmatrix} -i\Gamma\cos^2\phi & 0 & -i\Gamma\sin 2\phi/2 \\ 0 & 0 & 0 \\ i\Gamma\sin 2\phi/2 & 0 & -i\Gamma\sin^2\phi \end{bmatrix}.\end{aligned} \tag{4}$$

In Eq. (4), an over dot denotes the z-derivative. Here we have again used the perturbation approach and dropped the C_{13} terms for simplicity. It is clear that $\mathbf{H}_{adia}$ is not exactly diagonal despite the instantaneous eigenstate basis. However, if the system evolves slowly, the derivatives in the off-diagonal terms will vanish, and the modes are nearly decoupled. This particularly leads to isolation of the $|\Psi_0^{(0)}\rangle$ state, because its related elements in the perturbation matrix are zero. Therefore, near-lossless evolution within $|\Psi_0^{(0)}\rangle$ can be obtained, although the exact lossless limit requires infinite interaction length. Note that the $|\Psi_n^{(0)}\rangle$ states are the zeroth-order terms of the exact eigenstates of $\mathbf{H}$. The latter

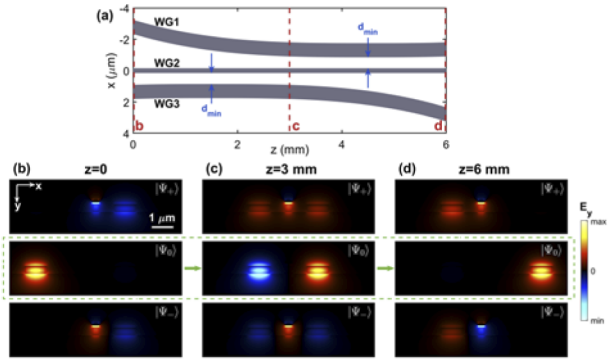

Fig. 2. (a) Layout of the three waveguides. (b)–(d) Electric field of the supermodes (instantaneous eigenstates) at the cross-section of (b) $z = 0$, (c) $z = 3$ mm, and (d) $z = 6$ mm. For the STIRAP-like transfer of the TM mode, the system evolves mainly in the $|\Psi_0^{(0)}\rangle$ state in the dashed box. For TE supermodes, see Supplement 1.

can be expressed by the perturbation theory to the first-order approximation:

$$|\Psi_n\rangle = |\Psi_n^{(0)}\rangle + \sum_{m\neq n} \frac{\langle \Psi_m^{(0)}| \mathbf{H}' |\Psi_n^{(0)}\rangle}{(\lambda_n^{(0)} - \lambda_m^{(0)})} |\Psi_m^{(0)}\rangle, m, n \in \{+, 0, -\}. \quad (5)$$

These exact eigenstates will be visualized in Figs. 2(b)–2(d).

To implement the STIRAP-like light transfer in a waveguide system, we consider the waveguide layout depicted in Fig. 2(a). The shapes of WG1 and WG3 are defined by $x_{\mathrm{WG1}}(z) = -a_0|z - z_{0\mathrm{WG1}}|^3 + d_{\min} + (w_{\mathrm{LN}} + w_{\mathrm{HPWG}})/2$ and $x_{\mathrm{WG3}}(z) = a_0|z - z_{0\mathrm{WG3}}|^3 + d_{\min} + (w_{\mathrm{LN}} + w_{\mathrm{HPWG}})/2$, respectively, where $x_{\mathrm{WG1}}(z)$ and $x_{\mathrm{WG3}}(z)$ measure the z-dependence of the center positions of WG1 and WG3. Here, $d_{\min} = 700$ nm is the minimum edge-to-edge distance, occurring at $z_{0\mathrm{WG1}} = 4.5$ mm for WG1 and $z_{0\mathrm{WG3}} = 1.5$ mm for WG3. The full device length is 6 mm. The coefficient affecting the degree of bending is $a_0 = 16.33$ when all variables are converted to the unit of meters. These shapes are designed to obtain super-Gaussian-shaped coupling coefficient profiles [see Fig. 3(a)]. Despite the noticeable bending in Fig. 2(a), the local directional angle between the waveguide axial direction and the z-axis is very small ($dx/dz = 0.001$ at maximum). Therefore, the refractive index change resulting from the propagation direction in X-cut LN is negligible.

This also makes it convenient to use the local normal mode representation to illustrate the TM mode evolution in the waveguide system, as presented in Figs. 2(b)–2(d). We used a two-dimensional (2D) finite difference mode solver (Lumerical MODE) to obtain the supermodes. The simulation wavelength is 1550 nm. The refractive indices of LN are 2.1379 (extraordinary) and 2.2112 (ordinary) [29], and the indices of gold and silicon dioxide are 0.5301 + 10.81i and 1.444, respectively. The supermodes are correlated to the adiabatic states in Eq. (5) [or Eq. (3) with zeroth-order approximation], because both representations depict the same eigenstates of $\mathbf{H}$. The evolution of these adiabatic modes during the field propagation can be clearly seen in Figs. 2(b)–2(d). Particularly, the $|\Psi_0\rangle$ state, which evolves from $|1\rangle$ into $|3\rangle$, is observed to be a dark state not involving WG2. This explains the near-lossless light transfer mechanism, even if a lossy HWPG is included in the system.

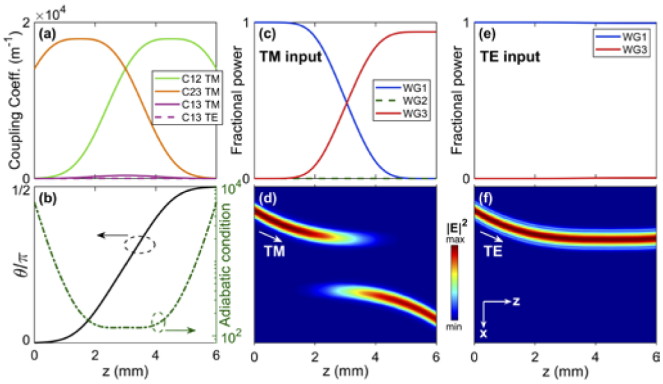

Fig. 3. (a) Coupling coefficient profile. Left to right: first curve, C23 TM; second curve, C12 TM. (b) Evolution of the parameter θ and the adiabatic condition. (c), (d) Propagation of a TM mode injected in WG1 by (c) CMT calculation (left to right: first curve, WG3, second curve, WG1) and (d) EME simulation. (e), (f) Same as in panels (c), (d) but for the TE mode.

To examine the performance of the proposed PBS, we conducted CMT calculations and 3D simulations using the eigenmode expansion (EME) method (Lumerical EME). For CMT, we extract the coupling coefficients between two waveguides following the derivations in [28]. The resultant coupling coefficient profiles along z are plotted in Fig. 3(a). Empirically, the coupling coefficient decays exponentially with the waveguide separation. Thus, $C_{12}(z)$ and $C_{23}(z)$ take the form of truncated third-order super-Gaussian functions resulting from the "reflected" cubic function profiles of WG1 and WG3. Such profiles are designed to optimize the overlap of the coupling strengths for STIRAP transfer. To provide guidance for the optimization, we plot two parameters in Fig. 2(b): the angle θ in Eq. (3) and an adiabatic condition parameter defined as $\sqrt{|C_{12}(z)|^2 + |C_{23}(z)|^2}/\dot{\theta}$. This parameter compares the diagonal elements (approximately $\sqrt{|C_{12}(z)|^2 + |C_{23}(z)|^2}$) in Eq. (4) to the off-diagonal elements (approximately $\dot{\theta}$) and estimates the degree of adiabaticity. It is evident in Fig. 3(b) that θ evolves smoothly from initial value 0 to final value $\pi/2$, which corresponds to $|1\rangle \rightarrow |3\rangle$, and the adiabatic condition number >100 holds for the entire propagation, indicating the transfer here is close to the adiabatic limit. We calculate the fractional power in the waveguides following Eq. (1) and Eq. (2).

The CMT result of the TM input from WG1 is shown in Fig. 3(c). A high transfer efficiency of 91.2% from WG1 to WG3 is achieved, and the residual power in WG1 is negligible (approximately 10^{-6}). The corresponding EME simulation is presented in Fig. 3(d). The simulated efficiency of 93.2%, extracted from the scattering matrix, is in good agreement with CMT. For the TE mode, the two-waveguide coupling can be expressed by

$$i\frac{d}{dz}\begin{bmatrix} a_{1\mathrm{TE}} \\ a_{3\mathrm{TE}} \end{bmatrix} = \begin{bmatrix} 0 & C_{13\mathrm{TE}}(z) \\ C_{13\mathrm{TE}}^*(z) & 0 \end{bmatrix} \begin{bmatrix} a_{1\mathrm{TE}} \\ a_{3\mathrm{TE}} \end{bmatrix}. \quad (6)$$

The calculated fractional power is plotted in Fig. 3(e). Owing to the small direct coupling coefficient between WG1 and WG3 [see Fig. 3(a)], the cross-coupling from WG1 to WG3 is <1% (−20 dB). This is also validated by the EME simulation in Fig. 3(f), which shows near unity transmission through WG1.

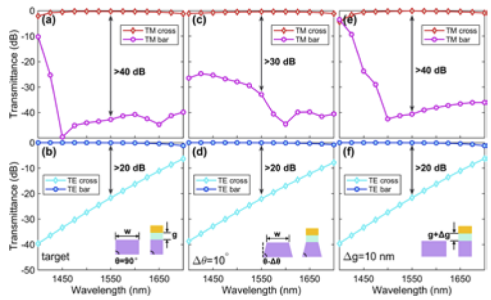

Fig. 4. Simulated transmittance spectra of the PBS with (a), (b) target parameters; (c), (d) slanted sidewalls ($\Delta\theta = 10°$); (e), (f) deviation of the thickness of the SiO_2 interlayer ($\Delta g = 10$ nm).

The transfers here are reciprocal, thus beam combining of TE and TM can also be obtained.

The STIRAP process can be understood as a single-mode evolution effect in its eigenmode basis (scaling with relative coupling strengths), rather than multimode interference (scaling with wavelength and device length [17,30]). As a result, our PBS exhibits a large bandwidth and good tolerance to fabrication imperfections. Figures 4(a) and 4(b) present the simulated bandwidth of the PBS with target parameters. The extinction of the TM mode transfer is <−40 dB over a bandwidth of approximately 250 nm (1450–1700 nm). The insertion loss is 0.3 dB at the design wavelength (1550 nm) and stays less than 1 dB for approximately the same bandwidth interval. The TE extinction is below −20 dB for wavelengths shorter than 1550 nm. A significant source of imperfection in LNOI fabrication technologies is slanted sidewalls. We have assumed 90° sidewalls for simplicity and also examined the case with 80° sidewalls ($\Delta\theta = 10°$) in Figs. 4(c) and 4(d). The extinction of TM (<−30 dB) is affected very slightly, whereas the bandwidth, in this case, can extend to even shorter wavelengths. Another delicate parameter is the height of the silicon dioxide interlayer in the HPWG. We show in Figs. 4(e) and 4(f) that Δg=10 nm would not affect the extinction at 1550 nm. In both cases, the effect of fabrication imperfections on the TE performance is minimal (for complete analysis, see Supplement 1).

In conclusion, we have investigated the photonic analogy of a STIRAP system involving a decaying intermediate state and proposed a novel design of integrated PBS. The STIRAP scheme enables broadband light transfer in a three-waveguide system via a plasmonic waveguide. The inherent losses from the plasmonic waveguide are circumvented thus achieving a low-loss broadband plasmonic PBS. We theoretically and numerically demonstrate a robust transfer (<−40 dB extinction) of the TM mode over approximately 250 nm bandwidth, covering the entire S-, C-, and L-bands and part of the E-band, with TE extinction <−20 dB for wavelengths <1550 nm. Moreover, an insertion loss of <1 dB almost throughout the bandwidth is achieved despite the presence of a plasmonic structure. Our proposed PBS facilitates the development of integrated photonic circuits.

Funding. Boston University and Reidy Career Award (AFOSR, FA9550-18-1-0056); U.S. Department of Defense Applied Research Laboratory (W911NF-20-2-012).

Disclosures. The authors declare no conflicts of interest.

Data availability. Data underlying the results presented in this paper are not publicly available at this time but may be obtained from the authors upon reasonable request.

Supplemental document. See Supplement 1 for supporting content.

REFERENCES

1. S. Longhi, Laser Photonics Rev. **3**, 243 (2009).
2. J. Kuklinski, U. Gaubatz, F. T. Hioe, and K. Bergmann, Phys. Rev. A **40**, 6741 (1989).
3. U. Gaubatz, P. Rudecki, S. Schiemann, and K. Bergmann, J. Chem. Phys. **92**, 5363 (1990).
4. E. Paspalakis, Opt. Commun. **258**, 30 (2006).
5. S. Longhi, Phys. Rev. E **73**, 026607 (2006).
6. S. Longhi, G. Della Valle, M. Ornigotti, and P. Laporta, Phys. Rev. B **76**, 201101 (2007).
7. R. Menchon-Enrich, A. Llobera, J. Vila-Planas, V. J. Cadarso, J. Mompart, and V. Ahufinger, Light: Sci. Appl. **2**, e90 (2013).
8. T. Lunghi, F. Doutre, A. P. Rambu, M. Bellec, M. P. De Micheli, A. M. Apetrei, O. Alibart, N. Belabas, S. Tascu, and S. Tanzilli, Opt. Express **26**, 27058 (2018).
9. C. W. Wu, A. S. Solntsev, D. N. Neshev, and A. A. Sukhorukov, Opt. Lett. **39**, 953 (2014).
10. J.-H. Park, A. Ndao, W. Cai, L. Hsu, A. Kodigala, T. Lepetit, Y.-H. Lo, and B. Kanté, Nat. Phys. **16**, 462 (2020).
11. L. Hsu, F. I. Baida, and A. Ndao, Opt. Express **29**, 1102 (2021).
12. E. J. Bergholtz, J. C. Budich, and F. K. Kunst, Rev. Mod. Phys. **93**, 015005 (2021).
13. S. Ke, D. Zhao, Q. Liu, and W. Liu, Opt. Quantum Electron. **50**, 1 (2018).
14. B. T. Torosov, G. Della Valle, and S. Longhi, Phys. Rev. A **89**, 063412 (2014).
15. N. Vitanov and S. Stenholm, Phys. Rev. A **56**, 1463 (1997).
16. D. Dai and S. He, Opt. Express **17**, 16646 (2009).
17. F. Lou, D. Dai, and L. Wosinski, Opt. Lett. **37**, 3372 (2012).
18. G. Ulliac, V. Calero, A. Ndao, F. Baida, and M.-P. Bernal, Opt. Mater. **53**, 1 (2016).
19. J. Zhao, C. Ma, M. Rüsing, and S. Mookherjea, Phys. Rev. Lett. **124**, 163603 (2020).
20. M. Mahmoud, L. Cai, C. Bottenfield, and G. Piazza, IEEE Photonics J. **10**, 1 (2018).
21. M. Reig Escalé, F. Kaufmann, H. Jiang, D. Pohl, and R. Grange, APL Photonics **5**, 121301 (2020).
22. Z. Gong, R. Yin, W. Ji, J. Wang, C. Wu, X. Li, and S. Zhang, Opt. Commun. **396**, 23 (2017).
23. C. Deng, M. Lu, Y. Sun, L. Huang, D. Wang, G. Hu, R. Zhang, B. Yun, and Y. Cui, Opt. Express **29**, 11627 (2021).
24. H. Xu, D. Dai, L. Liu, and Y. Shi, Opt. Express **28**, 10899 (2020).
25. P. Aashna and K. Thyagarajan, J. Opt. **19**, 065805 (2017).
26. H.-P. Chung, C.-H. Lee, K.-H. Huang, S.-L. Yang, K. Wang, A. S. Solntsev, A. A. Sukhorukov, F. Setzpfandt, and Y.-H. Chen, Opt. Express **27**, 1632 (2019).
27. R. Alrifai, V. Coda, A. A. Rangelov, and G. Montemezzani, Phys. Rev. A **100**, 063841 (2019).
28. W.-P. Huang, J. Opt. Soc. Am. A **11**, 963 (1994).
29. G. Edwards and M. Lawrence, Opt. Quantum Electron. **16**, 373 (1984).
30. N. Abadía, X. Dai, Q. Lu, W.-H. Guo, D. Patel, D. V. Plant, and J. F. Donegan, Opt. Express **25**, 10070 (2017).